EHD2-mediated restriction of caveolar dynamics regulates cellular fatty acid uptake

Claudia Matthaeus[a,1,2], Ines Lahmann[b,1], Séverine Kunz[c], Wenke Jonas[d,e], Arthur Alves Melo[a], Martin Lehmann[f,g], Elin Larsson[h], Richard Lundmark[h], Matthias Kern[i], Matthias Blüher[i], Hannah Olschowski[j], Julian Kompa[j], Britta Brügger[j], Dominik N. Müller[k,l], Volker Haucke[f,g,m], Annette Schürmann[d,e], Carmen Birchmeier[b], and Oliver Daumke[a,m,2]

[a]Crystallography, Max Delbrück Center for Molecular Medicine, 13125 Berlin, Germany; [b]Signal Transduction/Developmental Biology, Max Delbrück Center for Molecular Medicine, 13125 Berlin, Germany; [c]Electron Microscopy Core Facility, Max Delbrück Center for Molecular Medicine, 13125 Berlin, Germany; [d]Experimental Diabetology, German Institute of Human Nutrition Potsdam-Rehbruecke, 14558 Nuthetal, Germany; [e]Department of Experimental Diabetology, German Center for Diabetes Research, 85764 München-Neuherberg, Germany; [f]Department of Molecular Pharmacology and Cell Biology, Leibniz-Forschungsinstitut für Molekulare Pharmakologie, 13125 Berlin, Germany; [g]Imaging Core Facility, Leibniz-Forschungsinstitut für Molekulare Pharmakologie, 13125 Berlin, Germany; [h]Integrative Medical Biology, Umeå University, 901 87 Umeå, Sweden; [i]Department of Medicine, University of Leipzig, 04103 Leipzig, Germany; [j]Heidelberg University Biochemistry Center, University of Heidelberg, 69120 Heidelberg, Germany; [k]Experimental and Clinical Research Center, Charité Universitätsmedizin Berlin, 13125 Berlin, Germany; [l]Experimental and Clinical Research Center, Max Delbrück Center for Molecular Medicine, 13125 Berlin, Germany; and [m]Institute of Chemistry and Biochemistry, Freie Universität Berlin, 14195 Berlin, Germany

Edited by Joseph Albanesi, University of Texas, Dallas, TX, and accepted by Editorial Board Member David J. Mangelsdorf February 14, 2020 (received for review November 8, 2019)

Eps15-homology domain containing protein 2 (EHD2) is a dynamin-related ATPase located at the neck of caveolae, but its physiological function has remained unclear. Here, we found that global genetic ablation of EHD2 in mice leads to increased lipid droplet size in fat tissue. This organismic phenotype was paralleled at the cellular level by increased fatty acid uptake via a caveolae- and CD36-dependent pathway that also involves dynamin. Concomitantly, elevated numbers of detached caveolae were found in brown and white adipose tissue lacking EHD2, and increased caveolar mobility in mouse embryonic fibroblasts. EHD2 expression itself was down-regulated in the visceral fat of two obese mouse models and obese patients. Our data suggest that EHD2 controls a cell-autonomous, caveolae-dependent fatty acid uptake pathway and imply that low EHD2 expression levels are linked to obesity.

EHD2 ATPase | caveolae | fatty acid uptake | lipid metabolism | obesity

Caveolae are small membrane invaginations of the plasma membrane that are abundantly found in adipocytes and endothelial and muscle cells (1). They have been implicated in the regulation of membrane tension (2, 3), in mediating lipid metabolism (4), or in acting as distinct sites for specific and highly regulated signaling cascades, such as the endothelial nitric oxide synthase (eNOS)–nitric oxide (NO) pathway (5). The characteristically shaped caveolar bulb has a typical diameter of 50 to 100 nm and is connected to the cell surface via a narrow neck region. The integral membrane protein Caveolin (with three isoforms in human, Cav1 to -3) and the peripheral membrane protein Cavin (with four isoforms in human, Cavin1 to -4) build a mesh-like coat around the caveolar bulb (6–10). In addition, Bin/amphiphysin/Rvs domain-containing proteins of the PACSIN/syndapin family (PACSIN1 to -3 in human) participate in the biogenesis of caveolae (11–13).

Loss of Cav1/Cav3 or Cavin1 results in a complete lack of caveolae from the plasma membrane (4, 14, 15). Cav1 knockout (KO) mice suffer from cardiomyopathy, pulmonary hypertension, endothelium-dependent relaxation problems, and defective lipid metabolism (1). In agreement with the latter, Cav1 KO mice are resistant to high fat diet-induced obesity (16) and display smaller white adipocytes and fat pads (17). Furthermore, increased levels of triglycerides and fatty acids (FAs) are found in blood plasma samples obtained from Cav1 KO mice, suggesting a reduced cellular uptake of FAs (16). A similar metabolic phenotype was found in mice lacking Cavin1 (4, 18). Conversely, overexpression of Cav1 in adipocytes results in an increased number of caveolae, enhanced fat accumulation, enlarged adipocytes, and lipid droplets (LDs) (19). These results suggest that caveolae are involved in lipid accumulation in adipocytes and may promote FA uptake (20). However, the molecular mechanisms of caveolae-dependent fat uptake have remained obscure.

Eps15 homology domain containing protein 2 (EHD2) localizes to the caveolar neck region (6, 21, 22). The protein belongs to the dynamin-related EHD ATPase family, which comprises four members in human (EHD1 to -4), and shows strong expression in human adipose and muscle tissue (human protein atlas) (23). EHD2 is built of an N-terminal GTPase (G)-domain, which mediates dimerization and oligomerization, a helical domain containing the membrane binding site, and a C-terminal regulatory Eps15 homology (EH)-domain. The proteins exist in a closed auto-inhibited conformation in solution (24). When recruited to membranes, a series of conformational changes align the phospholipid binding sites with the membrane and

Significance

Caveolae are small plasma membrane invaginations that are particularly abundant in adipocytes. Caveolae are implicated in lipid uptake, but the exact mechanism is not clear. Here, we characterized the physiological function of EHD2, a protein that is found at the neck of caveolae. We established a link between higher caveolar mobility induced by EHD2 loss and increased cellular fatty acid uptake. Concurrently, lipid droplets were enlarged in various tissues of EHD2-lacking mice. Our data suggest that EHD2 controls a cell-autonomous, caveolae-dependent fatty acid uptake pathway. Notably, obese patients express only low levels of EHD2, implicating a role of EHD2-controlled caveolar dynamics in obesity.

Author contributions: C.M., I.L., S.K., W.J., A.A.M., M.L., R.L., M.B., B.B., D.N.M., V.H., A.S., C.B., and O.D. designed research; C.M., I.L., S.K., W.J., A.A.M., M.L., E.L., M.K., H.O., and J.K. performed research; C.M., I.L., M.L., M.K., and M.B. contributed new reagents/analytic tools; C.M., I.L., S.K., W.J., A.A.M., M.K., M.B., H.O., J.K., B.B., D.N.M., V.H., A.S., C.B., and O.D. analyzed data; and C.M., R.L., V.H., A.S., and O.D. wrote the paper.

The authors declare no competing interest.

This article is a PNAS Direct Submission. J.A. is a guest editor invited by the Editorial Board.

[1]C.M. and I.L. contributed equally to this work.

[2]To whom correspondence may be addressed. Email: claudia.matthaeus@nih.gov or oliver.daumke@mdc-berlin.de.

This article contains supporting information online at https://www.pnas.org/lookup/suppl/doi:10.1073/pnas.1918415117/-/DCSupplemental.

First published March 13, 2020.

facilitate oligomerization of EHD2 into ring-like structures (25–27).

Down-regulation of EHD2 in cell culture results in decreased surface association and increased mobility of caveolae whereas EHD2 overexpression stabilizes caveolae at the plasma membrane (9, 21, 22, 28). This led to the hypothesis that formation of an EHD2-ring at the neck of caveolae restricts caveolar mobility within the membrane. In agreement with this hypothesis, EHD2 assembles in an ATP-dependent fashion into ring-like oligomers in vitro and induces the formation of tubular liposomes with an inner diameter of 20 nm, corresponding to the diameter of the caveolar neck (24). Whether EHD2 also controls caveolar membrane dynamics in vivo and what the physiological consequences of EHD2 loss at the organismic level are is unknown.

In this study, we found that EHD2 KO mice display enlarged LDs in white and brown adipose tissue (WAT/BAT) and in caveolae-containing cell types, like adipocytes or fibroblasts, although total cellular triglyceride levels were not altered. In adipose tissue lacking EHD2, caveolae were frequently detached from the plasma membrane and displayed elevated mobility. Furthermore, in two obesity mouse models, as well as in white adipose tissue (WAT) of obese patients, reduced EHD2 expression and an increased number of detached caveolae were found in visceral fat. Our data establish EHD2 as a negative regulator of caveolae-dependent lipid uptake and implicate a role of caveolar stability and dynamics for lipid homeostasis and obesity.

Results

Generation of EHD2 Knockout Mice. To examine the physiological function of EHD2, a mouse strain with LoxP recognition sites surrounding exon 3 and intron 3 of the *Ehd2* gene was engineered (Fig. 1*A*). Exon 3 encodes residues 137 to 167 of the highly conserved GTPase domain, and its deletion is predicted to result in nonfunctional protein. Following global removal of exon 3 by crossings with a germ line-specific Cre-deleter strain, offspring mice were back-crossed with the C57BL6/N mouse strain for five generations, yielding a global EHD2 KO mouse model. Genotyping of offspring confirmed the successful deletion (del) of EHD2 exon 3 in EHD2 del/del animals (*SI Appendix*, Fig. S1*A*), and real-time PCR revealed the absence of EHD2 messenger RNA (mRNA) in the EHD2 del/del tissue (Fig. 1*B*). Western blot analysis indicated the complete loss of EHD2 in WAT and various other tissues of EHD2 del/del mice compared to abundant EHD2 expression in EHD2 +/+ and del/+ mice (Fig. 1*C* and *SI Appendix*, Fig. S1 *B–D*). Cav1 and Cavin1 protein levels remained grossly unaltered upon loss of EHD2 (Fig. 1*C* and *SI Appendix*, Fig. S1*D*). Accordingly, immunostaining of cryostat sections obtained from EHD2 del/del BAT did not reveal apparent differences in Cav1 or Cavin1 expression and localization (*SI Appendix*, Fig. S1*E*) whereas EHD2 staining was completely abolished (Fig. 1*D*).

Loss of EHD2 Results in Increased Lipid Droplet Size. EHD2 del/del mice were born in normal Mendelian ratios, were fertile, and did not show an obvious phenotype upon initial inspection. In contrast to the reported loss of white fat mass in Cav1 and Cavin1 KO mouse models (4, 16, 17), 1-y-old EHD2 del/del male mice were not apparently lipodystrophic and did not display any detectable weight difference when compared to EHD2 del/+ mice (Fig. 1*E*). However, several of the EHD2 del/del mice showed increased deposits of epigonadal and peri-inguinal white fat (Fig. 1*F*). This suggested that loss of EHD2 led to a more subtle phenotype, such as the dysregulation of lipid storage capacity.

When analyzed at the cellular level, white adipocytes of EHD2 del/del mice showed an increased cell size compared to adipocytes from EHD2 del/+ mice or adult C57BL6/N mice (Fig. 1*G* and *SI Appendix*, Fig. S2*A*). In contrast to EHD2 del/+ BAT with its distinct brown appearance, EHD2 del/del BAT showed increased beige and white coloring (Fig. 1*H*). Histological inspections of BAT paraffin and cryostat sections stained against the LD coat protein Perilipin1 indicated an increased LD size in EHD2 del/del BAT compared to EHD2 del/+ or C57BL6/N mice (Fig. 1*H* and *SI Appendix*, Fig. S2 *B* and *C*). Concurrently, the number of LDs in brown adipocytes was reduced in cells lacking EHD2 (Fig. 1*I*). Despite their enlarged sizes, we did not observe an abnormal LD shape in brown adipocytes from EHD2 del/del mice compared to EHD2 del/+ by electron microscopy (EM) and light microscopy analysis (*SI Appendix*, Fig. S3). Thus, LDs in EHD2 del/del brown adipocytes showed an apparently normal shape and protein coat and regular contact sites with mitochondria (*SI Appendix*, Fig. S3 *A–D*). Based on mass spectrometry analysis (29), it was previously proposed that EHD2 is partially associated with LDs. However, immunostainings of mouse embryonic fibroblasts (MEFs) revealed EHD2 rarely at LDs, as reflected by Pearson correlation analysis (*SI Appendix*, Fig. S3 *E* and *F*). As no significant differences in lipid accumulation were found in EHD2 del/+ and C57BL6/N male mice (*SI Appendix*, Fig. S2) and to reduce animal numbers, the following experiments were carried out with EHD2 del/+ as control group to EHD2 del/del male mice.

Based on the increased LD sizes in EHD2-lacking adipocyte tissue, we further investigated if the lipid content and adipocyte differentiation was altered in EHD2 del/del WAT and BAT. However, similar diacyl- and triacylglyceride concentrations were found in EHD2 del/+ and del/del WAT and BAT (Fig. 1 *J* and *K* and *SI Appendix*, Fig. S2*D*), in agreement with the similar weight of EHD2 del/del and del/+ mice. Total cholesterol and cholesterol esters were slightly increased in EHD2 del/del BAT, but not in WAT (Fig. 1 *L* and *M*). In addition, we did not detect any significant differences in adiponectin, leptin, and insulin plasma levels in EHD2 del/del compared to del/+ mice (*SI Appendix*, Fig. S4). Free FA concentrations in blood plasma were slightly reduced in EHD2 del/del, in line with a possible increase in cellular FA uptake (*SI Appendix*, Fig. S4). Adipogenic marker genes like PPARγ, Retn, or Serpina3k displayed a slightly increased expression in EHD2 del/del WAT or differentiated primary adipocytes compared to EHD2 del/+ (*SI Appendix*, Fig. S5*A*), indicating that differentiation was not altered. Contrarily, we observed a decreased expression of genes involved in de novo lipogenesis in isolated WAT obtained from EHD2 del/del vs. EHD2 del/+ mice or in primary adipocyte cell cultures (*SI Appendix*, Fig. S5*B*), suggesting that down-regulation of lipogenesis is an active mechanism that partially compensates for the increased lipid accumulation. However, EHD2 del/del WAT or adipocytes showed increased expression of proteins involved in LD biogenesis [e.g., DGAT2, Perilipin1, and Lipin1 (*SI Appendix*, Fig. S5*C*)] and FA activation, such as Acyl-CoA Synthetase Long Chain Family Member 3 and -4 (*SI Appendix*, Fig. S5*D*). In summary, the absence of EHD2 leads to decreased expression levels of genes involved in de novo fat metabolism and increased expression levels of genes associated with the synthesis of LDs.

Increased Rates of Lipid Uptake in Adipocytes Lacking EHD2. To characterize the mechanism of increased LDs in EHD2 del/del fat cells, lipid metabolism was investigated in cultured adipocytes. Primary preadipocytes were isolated from WAT of EHD2 del/+ and EHD2 del/del mice and differentiated into mature adipocytes, followed by boron dipyrromethene (BODIPY) staining to label LDs. Undifferentiated EHD2 del/del preadipocytes showed increased LD size compared to EHD2 del/+ preadipocytes, a difference that was even more pronounced in differentiated adipocytes (Fig. 2 *A* and *B*). Three-dimensional (3D) reconstructions of EHD2 del/del differentiated adipocytes illustrated an extensively increased volume of some LDs in del/del differentiated adipocytes (Fig. 2*C*).

We addressed the possibility that increased lipid uptake is a secondary effect of EHD2 deletion mediated via putative organ

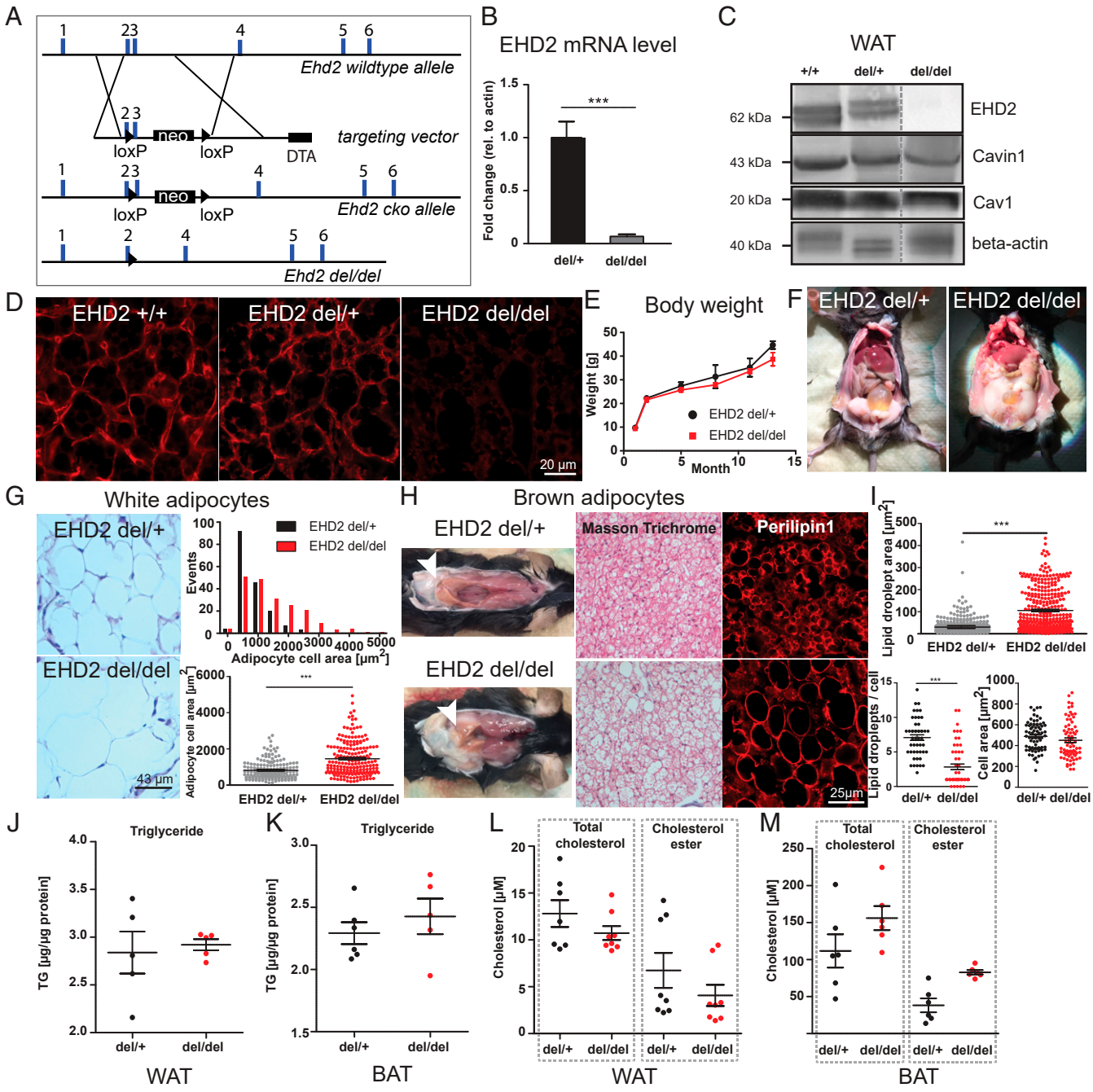

Fig. 1. Loss of EHD2 results in increased lipid accumulation in white and brown adipose tissue. (*A*) Generation of the EHD2 KO mouse model. A targeting vector containing a pGK-Neomycin (neo) cassette and loxP sites flanking exon 3 was placed in the EHD2 wild-type allele. EHD2 del/del mice were obtained by breeding with Cre-deleter mouse strain (diphtheria toxin A [DTA]). (*B*) EHD2 mRNA level in EHD2 del/+ and EHD2 del/del mice (mRNA from BAT, $n = 5$). (*C*) Western blot analysis of WAT of EHD2 +/+, $^{+/-}$, and $^{-/-}$ mice against EHD2, Cav1, and Cavin1. (*D*) EHD2 immunostaining in BAT cryostat sections from EHD2 +/+, del/+, and del/del mice. (*E*) The body weight was monitored over 12 mo ($n = 7$). (*F*) EHD2 del/+ and EHD2 del/del mice during preparation. (*G*) Masson trichrome staining of WAT paraffin sections of EHD2 del/+ and EHD2 del/del. Analysis of the adipocyte cell size [n(del/+) = 172/3, n(del/del) = 199/3]. (*H*) EHD2 del/del mice showed increased amount of beige BAT in the neck region. In addition, white adipocytes were infiltrated into the BAT depots (white arrowheads). (*Left*) Masson trichrome staining of EHD2 del/+ and del/del BAT paraffin sections. (*Right*) BAT cryostat sections were stained against the LD coat protein Perilipin1 to visualize LDs. (*I*) LD size, number per cell, and cell area were measured in BAT cryostat sections [n(del/+) = 118/3, n(del/del) = 104/3]. (*J–M*) Triglyceride (TG; *J* and *K*), total cholesterol, and cholesterol ester (*L* and *M*) concentrations were determined for WAT ($n = 5$ to 8) and BAT ($n = 5$ to 6) of EHD2 del/+ and del/del mice. Line graph represents mean ± SE, column bar graphs show mean + SE or each replicate with mean ± SE, normal distributed groups were analyzed by *t* test, not normally distributed values with Mann–Whitney *U* test, $*P < 0.05$, $***P < 0.0001$. For comparison to C57BL6/N, see also *SI Appendix*, Figs. S1 and S2.

cross-talk. We therefore repeated the experiments with cultured adipocytes derived from EHD2 conditional knockout (cKO) flox/flox mice, in which EHD2 expression was down-regulated by expression of Cre recombinase via viral transfection. Again, EHD2 removal led to increased LD growth (*SI Appendix*, Fig. S6 *A* and *B*), indicating a cell-autonomous function of EHD2 in controlling lipid uptake.

A previous study suggested that EHD2 knock-down leads to impaired adipogenic differentiation in 3T3-L1 cells, and, as a

consequence, to smaller LDs (30). However, we reproduced our observation of increased LD sizes induced by the loss of EHD2 also in 3T3-L1 cells, even if we followed the published differentiation and EHD2 knockdown protocol (*SI Appendix*, Fig. S6 *C–H*). As already observed in EHD2-lacking BAT, the number of LDs was reduced in EHD2-knockout adipocytes (Fig. 2*D*).

LD growth can be mediated by the uptake of extracellular FAs and their conversion into triglycerides whereas glucose uptake and de novo lipogenesis play minor roles in this process (31, 32). FAs and lipids are present at high concentrations in fetal bovine serum (FBS). Addition of delipidated FBS during adipocyte differentiation resulted in complete loss of LDs in both genotypes (*SI Appendix*, Fig. S6 *I* and *J*) whereas glucose depletion led to a general impairment of adipocyte differentiation. Importantly, enlarged LDs were still observed in KO adipocytes, even under conditions of glucose depletion (*SI Appendix*, Fig. S6 *I* and *J*). These data led us to hypothesize that the increased LD size in EHD2 del/del adipocytes may be a consequence of increased FA uptake, in line with the suggested function of caveolae in FA uptake (33–35).

To test this possibility directly, we monitored the uptake of extracellularly added FAs into differentiated adipocytes using BODIPY-labeled dodecanoic acid (FA12) paired with fluorescence-activated cell sorting (FACS) analysis. After 5 min, only a minor fraction of EHD2 del/+ adipocytes displayed intense BODIPY staining (R2; for definition, see Fig. 2*E*). This R2 population increased to more than 30% after 60 min of BODIPY-FA12 treatment (Fig. 2 *E* and *F* and *SI Appendix*, Fig. S6 *K* and *L*). EHD2 del/del adipocytes displayed increased BODIPY staining at both early and late time points, indicating accelerated FA uptake (Fig. 2 *E* and *F* and *SI Appendix*, Fig. S6 *K* and *L*). This conclusion was further supported by light microscopy imaging, which revealed more intense BODIPY staining of EHD2 del/del compared to EHD2 del/+ adipocytes after 60 min of FA incubation (*SI Appendix*, Fig. S6*M*). In contrast, EHD2 del/+ and EHD2 del/del adipocytes did not differ with respect to their ability to take up extracellularly added glucose (*SI Appendix*, Fig. S6 *N–P*). Previously, an involvement of EHD2 in the autophagic engulfment of LDs (lipophagy) was suggested (36). However, inducing starvation by incubation of differentiated adipocytes with Hanks' balanced salt solution (HBSS) revealed no differences in the release of stored lipids in EHD2 del/+ and EHD2 del/del adipocytes, and both genotypes displayed similar reductions in lipid accumulation (*SI Appendix*, Fig. S6*Q*). These data indicate that loss of EHD2 does not affect the release of FAs or lipophagy but specifically controls LD size by regulating FA uptake.

Loss of EHD2 Results in Detachment of Caveolae from the Plasma Membrane In Vivo. Given the described role of caveolae in the uptake of FAs (16), we hypothesized that EHD2 may restrict FA uptake by controlling caveolar function. To test whether loss of EHD2 affects caveolar morphology, WAT and BAT were analyzed by electron microscopy (EM). Caveolae in EHD2 del/+ BAT were mostly membrane-bound and displayed the characteristic flask-shaped morphology (Fig. 3*A*, white arrowheads, ratio detached/membrane bound caveolae = 0.27). Strikingly, an increased number of caveolae appeared detached from the plasma membrane in BAT isolated from EHD2 del/del mice compared to EHD2 del/+ controls, as judged from the complete closure of the lipid bilayer in the plasma membrane and the caveolae (Fig. 3 *A*, white arrowheads, and *B*, ratio detached/membrane bound caveolae = 1.75). The total number of caveolae, as well as the caveolar diameter and size, was unchanged in brown adipocytes lacking EHD2.

An increased number of detached caveolae were also observed in EHD2 del/del white adipocytes compared to EHD2 del/+ cells from littermate controls (Fig. 3 *C*, black and white arrowheads, and *D*, ratio detached/membrane bound caveolae [del/del] = 1.2 vs. ratio [del/+] = 0.24). In white adipocytes, the total number of caveolae was reduced while both caveolar size and diameter were increased in EHD2 del/del compared to EHD2 del/+ animals (Fig. 3*D*). Cav1 immunogold labeling confirmed that the round vesicles close to the plasma membrane, indeed, were detached caveolae (Fig. 3*E*). The 3D visualization of EHD2 del/del brown adipocyte by electron tomography (ET) further indicated that the majority of detached caveolae in two-dimensional EM images were not connected to the plasma membrane (Fig. 3 *F* and *G* and Movie S1) but localized 20 to 30 nm underneath (Fig. 3 *G*, *a–c*) although some caveolae close to the plasma membrane showed thin connections (Fig. 3 *G*, *b* and *d*, white arrowhead). Taken together, EM and ET reveal an increased detachment of caveolae from the plasma membrane in EHD2 del/del adipocytes, suggesting a crucial function for EHD2 in the stabilization of caveolae at the plasma membrane.

Increased Caveolar Mobility in EHD2 Knockout Cells. To further dissect the interplay of caveolar mobility and LD growth at the molecular level, we investigated caveolar mobility and endocytosis in mouse embryonic fibroblasts (MEFs) by total internal reflection fluorescence (TIRF) microscopy. MEFs derived from EHD2 +/+ and del/del mice were transfected with a plasmid expressing Cav1 fused to enhanced green fluorescence protein (pCav1-EGFP) to label single caveolae. As illustrated in Fig. 4*A*, regions of moderate Cav1 expression were investigated to ensure that distinct Cav1 spots were observed during the analysis. Live TIRF imaging of EHD2 +/+ MEFs showed a slow or no continuous movement for the majority of investigated caveolae (Movie S2). However, single caveolae moved along the plasma membrane or left the TIRF illumination zone toward the inside of the cell, indicating their spontaneous detachment, as previously reported (21). Strikingly, movement and velocity of caveolae were greatly increased in EHD2 del/del MEFs (Movie S3), not allowing Cav1 single spots to be tracked. Line scan analysis revealed a greatly reduced number of fixed, nonmoving Cav1 spots (referred to as lines in Fig. 4*B*) in EHD2 del/del MEFs compared to EHD2 +/+ cells. Moreover, a larger number of highly mobile Cav1 sparks, reflecting fast moving caveolae, were found in EHD2 del/del cells (Fig. 4 *A* and *B*). Reexpression of EHD2 in EHD2 del/del MEFs reduced the mobility of caveolae, often leading to their immobilization (*SI Appendix*, Fig. S7 *A* and *B* and Movie S4).

Determinants of EHD2-Mediated Fatty Acid Uptake. We further characterized the determinants of FA uptake in MEFs. Similar to EHD2 del/del adipocytes, EHD2 del/del MEFs showed increased lipid accumulation and LD size after adipogenic differentiation or 6 h oleic acid treatment, as illustrated by LD BODIPY staining (*SI Appendix*, Fig. S8 *A* and *B*). Furthermore, the total number of LDs was reduced in EHD2 del/del MEFs after 6 h oleic acid treatment although the cell size was not altered (*SI Appendix*, Fig. S8 *C* and *D*). Compared to EHD2 +/+ MEFs, cholesterol and cholesterol ester concentrations were slightly increased in MEFs lacking EHD2 (*SI Appendix*, Fig. S8*E*), as already observed in EHD2 del/del BAT. Triglyceride levels were marginally reduced in EHD2 del/del MEFs (*SI Appendix*, Fig. S8*F*), probably due to the lower number of LDs found in EHD2 del/del cells. Notably, free fatty acid levels were similar in untreated EHD2 +/+ and del/del cells (*SI Appendix*, Fig. S8*G*). However, short-term (1 h) and, even more pronounced, long-term (24 h) exposure to oleic acid led to increased free fatty acid concentrations in EHD2 del/del cells (*SI Appendix*, Fig. S8*G*).

Reexpression of an EGFP-tagged EHD2 version in EHD2 +/+ and del/del MEFs rescued the observed LD phenotype, even reducing the size of LDs compared to EGFP expressing cells (Fig. 5 *A* and *B*). These data indicate a general and cell autonomous role of EHD2 in the control of LD growth and size that is not restricted to fat cells.

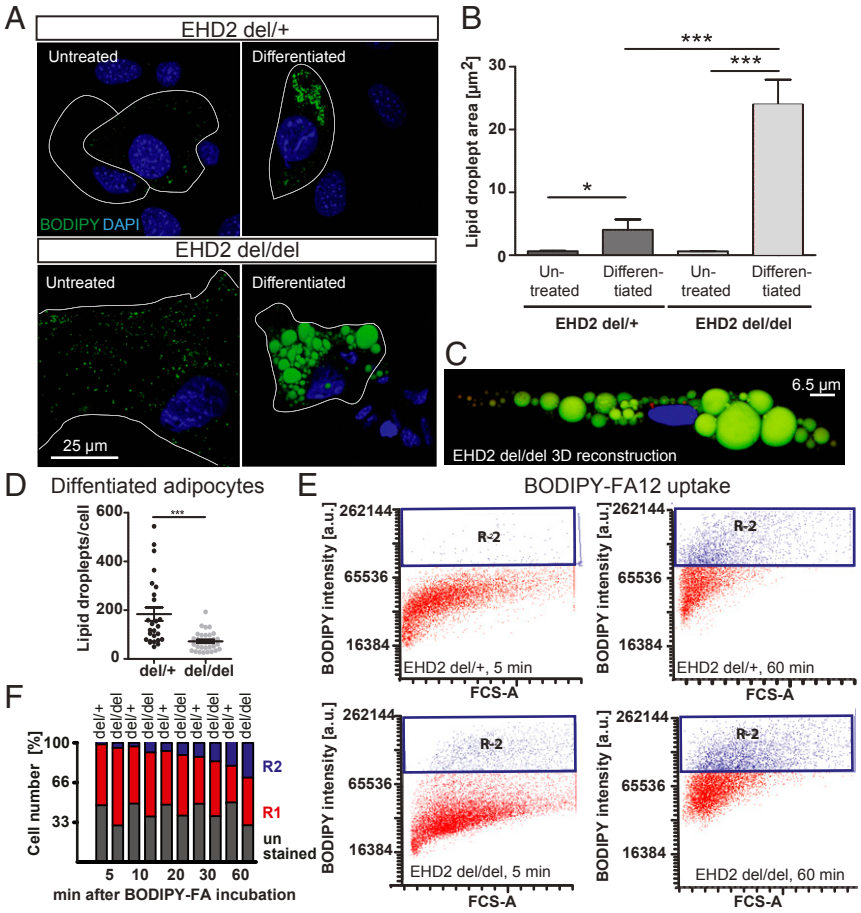

Fig. 2. EHD2 del/del adipocytes show increased LD size and faster fatty acid uptake. (*A–D*) Analysis of LD size in EHD2 del/del and EHD2 del/+ adipocytes by staining with BODIPY (*A* and *B*) [untreated: n(del/+) = 74/3, n(del/del) = 60/3); differentiated: n(del/+) = 132/3, n(del/del) = 95/3]. A 3D reconstruction of EHD2 del/del differentiated adipocyte (*C*). Green, LDs; blue, nucleus. (*D*) LD number per cell of differentiated EHD2 del/+ and del/del adipocytes [*H*, n(del/+) = 26/3; n(del/del) = 31/3]. (*E* and *F*) FA uptake assay in differentiated EHD2 del/+ and EHD2 del/del adipocytes was measured by FACS analysis. The R1 population indicates positively stained cells (illustrated in red in graph *E*). R2 populations correspond to higher BODIPY staining intensity in cells and represent adipocytes with increased BODIPY-FA12 uptake (shown in blue in *E*). The percentages of R1 and R2 cell numbers are shown in *F*. See also *SI Appendix*, Fig. S6. Column bar graphs illustrate mean ± SE, or each replicate with mean ± SE. A *t* test or Mann–Whitney *U* test was used to calculate significance, $*P < 0.05$; $***P < 0.0001$. a.u., arbitrary unit; FCS-A, forward cytometry standard-area.

To identify the functional regions within EHD2 that are crucial for regulating lipid uptake, we transfected EHD2 del/del MEFs with various EGFP-tagged EHD2 deletion constructs. EHD2 constructs lacking the N terminus, the EH-domain, or both rescued EHD2 loss, resulting in smaller LDs (*SI Appendix*, Fig. S8 *H* and *I*). In contrast, expression of single EHD2 mutants affecting membrane binding (F322A) or oligomerization/ATPase activity of EHD2 (F122A) did not reduce LD size, indicating a crucial role of these properties for EHD2 function.

To analyze if the observed phenotype in EHD2 del/del MEFs was dependent on caveolae, MEFs lacking EHD2 were treated with Cav1 or Cavin1 small interfering RNA (siRNA) (*SI Appendix*, Fig. S8 *J* and *K*) to eliminate caveolae. LD size in EHD2 del/del MEFs was significantly decreased following depletion of Cav1 or Cavin1 (Fig. 5*C*), indicating that the effects of EHD2 on LD size require, and likely are mediated by, caveolae.

It was previously reported that dynamin localizes to caveolae (37). Indeed, dynamin was observed in close proximity to Cav1 in immunostaining of MEFs, indicated by similar fluorescence intensity plot profiles (*SI Appendix*, Fig. S7*C*). Consistent with a role of dynamin in caveolae function, overexpression of a dynamin 2 dominant-negative mutant (pGFP-Dyn2-K44A) completely abolished the fast caveolar mobility in EHD2-lacking cells (*SI Appendix*, Fig. S7 *D–F* and Movies S5 and S6). Consequently, overexpression of the K44A mutant prevented increased LD size in EHD2 del/del MEFs (Fig. 5 *D* and *E*), pointing again to a link between caveolar mobility and FA uptake.

Previous work has implicated the FA binding membrane protein CD36 in caveolae-dependent FA uptake (33, 38, 39). To test whether CD36 is found in caveolae, we performed CD36 immunostaining of unfixed MEFs to preserve membrane structures. Indeed, CD36 partly colocalized with Cav1, indicating an accumulation of CD36 within caveolae (*SI Appendix*, Fig. S9*A*). However, we also observed CD36 in noncaveolar plasma membrane domains. Interestingly, correct CD36 plasma membrane localization depends on Cav1 expression as knockdown of Cav1 by three independent siRNAs revealed a decrease in CD36 antibody staining (*SI Appendix*, Fig. S9 *B–D*).

To probe a possible function of CD36 in EHD2-dependent lipid uptake, CD36 expression in MEFs was down-regulated by treatment with either one of three specific CD36 siRNAs. Antibody staining confirmed the efficient knockdown of CD36 in EHD2 +/+ and del/del MEFs (Fig. 5*F*). Removal of CD36 in EHD2 +/+ and del/del MEFs dramatically decreased the size of LDs compared to control siRNA-treated cells (Fig. 5 *F* and *G*). Hence, the observed enlargement of LDs in cells lacking EHD2 depends on CD36. These converging lines of evidence suggest that caveolae dynamics

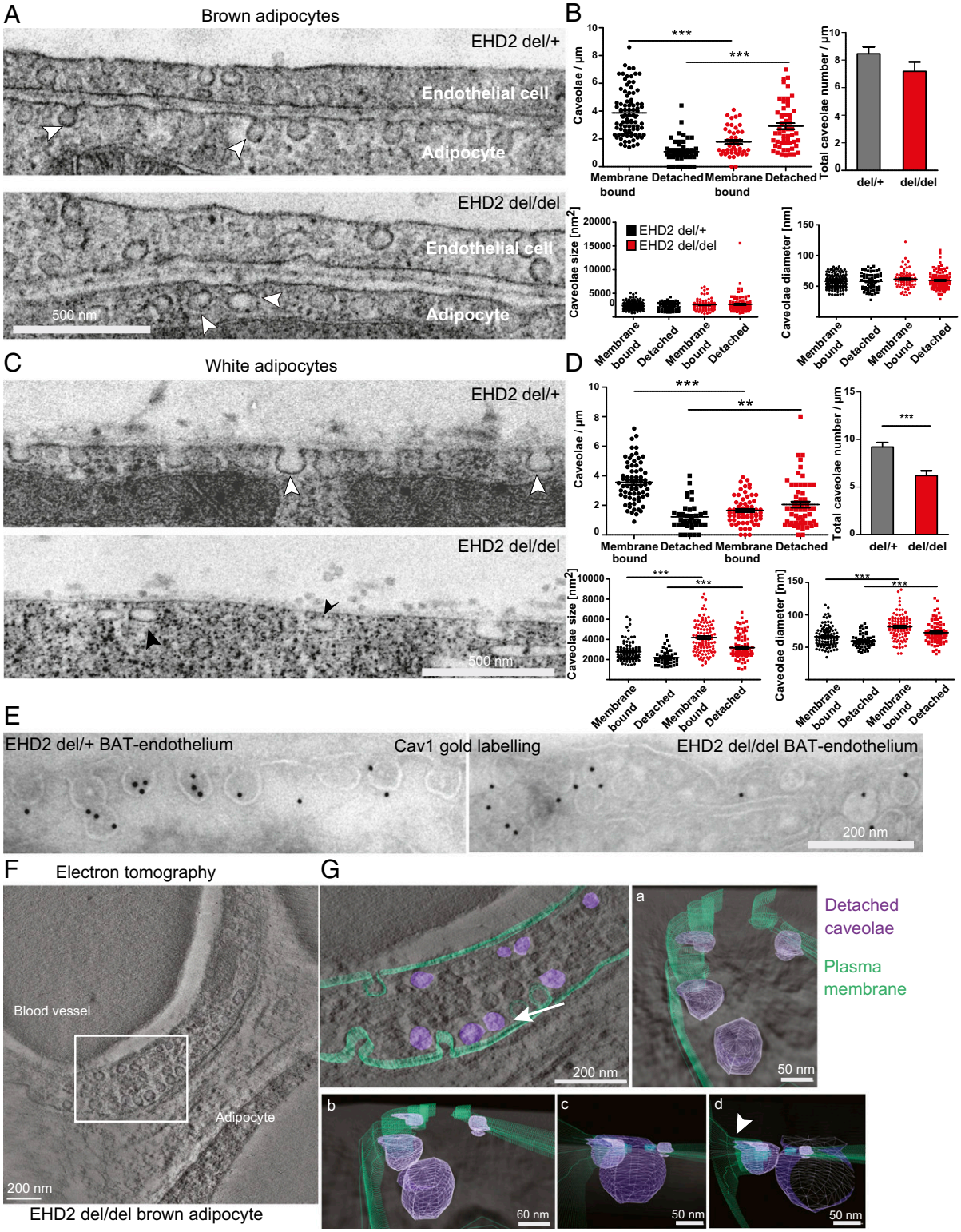

Fig. 3. Loss of EHD2 results in detached caveolae in vivo. (*A* and *B*) Representative EM images of BAT from EHD2 del/+ and del/del mice and systematic analysis [caveolae number: n(del/+) = 140/3, n(del/del) = 100/3; caveolae size and diameter: n(del/+) = 201/3, n(del/del) = 171/3]. White arrowheads indicate caveolae. (*C* and *D*) EM images of EHD2 del/+ and del/del WAT [caveolae number: n(del/+) = 108/3, n(del/del) = 124/3; caveolae size and diameter: n(del/+) = 151/3, n(del/del) = 185/3]. White arrowheads indicate membrane-bound caveolae, black arrowheads detached caveolae. (*E*) Representative image for EM gold immunolabeling against Cav1. Control labeling did not reveal specific staining. (*F* and *G*) Electron tomogram of a 150-nm EHD2 del/del BAT section (*F*). White box indicates segmentation and visualization of displayed cell area in *G*. The 3D model contains the plasma membrane (*G*, green) and the detached caveolae (violet). Detachment of caveolae was observed by changing the viewing angle (white arrow indicates the direction). Closer inspection of cell membrane and caveolae showed displacement of caveolae from the membrane. The 3D model also revealed attachment of some caveolae to the membrane (arrowhead). Graphs illustrate each replicate with mean ± SE; column bar graphs illustrate mean + SE. A *t* test or Mann–Whitney *U* test was used to calculate significance, $^{**}P < 0.001$; $^{***}P < 0.0001$. See also Movie S1.

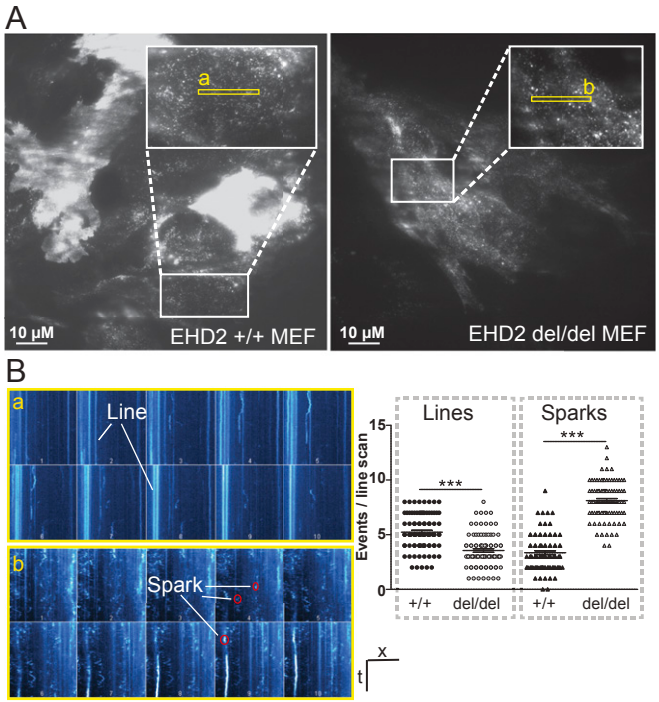

Fig. 4. Enhanced caveolar mobility in cells lacking EHD2. (*A* and *B*) TIRF live-imaging of EHD2 +/+ and del/del MEFs expressing pCav1-EGFP (in *A*, white boxes indicate magnified cell areas in which regions of interest, illustrated in yellow boxes, were analyzed). Line scan analysis of the recorded Cav1 intensities revealed for fixed, nonmoving caveolae lines and for fast moving caveolae single sparks (as illustrated in *a* and *b*). n($^{+/+}$) = 90/3; n(del/del) = 92/3; each replicate is represented with mean ± SE, ***$P < 0.0001$. t, time; x, scale; numbers 1–10 in single line scan panels indicate successive regions within the yellow rectangles. See also *SI Appendix*, Fig. S7 and Movies S2–S4.

is key to the regulation of FA internalization and that this is coupled to the previously shown roles of CD36 and caveolin.

Fatty Acid Trafficking Is Partially Mediated by Caveolae. The increased LD growth in EHD2 del/del MEFs suggests an FA trafficking route from the plasma membrane into the endoplasmic reticulum (ER) and, subsequently, to LDs. To further characterize this pathway, we followed the uptake of BODIPY-labeled FAs by time-resolved microscopy. TIRF live imaging showed fast FA intercalation into the plasma membrane of EHD2 +/+ and del/del MEFs (Fig. 6*A* and Movies S7 and S8). Concomitant with FA enrichment at the cell surface, we observed FA accumulation in single caveolae (Fig. 6*B*). Time-resolved tracking analysis indicated that FAs were also incorporated into mobile caveolae (Fig. 6*C* and Movies S9 and S10).

Next, we investigated the intracellular FA trafficking by confocal microscopy in fixed MEFs to identify the involved organelles. Within 1 min of FA treatment in EHD2 +/+ and del/del MEFs, labeled FAs were found inside the cell (Fig. 6 *D* and *E*). Both EHD2 +/+ and del/del MEFs showed FA trafficking into the ER. Cav1 gene silencing did not alter initial FA accumulation in the membrane and ER, suggesting that caveolae are not involved in the fast FA uptake step. After 3 min, labeled FAs were already found in LDs (see arrowheads in Fig. 6 *D* and *E*; also, see *SI Appendix*, Fig. S10*A*). Within 5 to 10 min of treatment, ER and LDs were intensively stained.

To analyze the caveolae dependence of this process, we quantified internalized cellular FAs by fluorescence intensity measurements (Fig. 6 *F* and *G*). Caveolae-dependent FA uptake was apparent after 10 min in EHD2 +/+ MEFs. Strikingly, in the absence of EHD2, caveolae-dependent FA uptake was already observed after 3 min and persisted to 10 min. Thus, cellular FA uptake follows an initial fast uptake route that is not dependent on caveolae, and a slower, caveolae-dependent uptake route that is modified by EHD2. Further FA processing steps, such as incorporation of FAs in diacylglycerol (DAG) followed by triacylglycerol conversion, were investigated by thin-layer chromatography (TLC) and lipid-based mass spectrometric (MS) analysis. Within 10 min of BODIPY-labeled FA (C12) treatment, BODIPY-positive DAG species were detected by TLC in EHD2 +/+ and del/del MEFs (*SI Appendix*, Fig. S10*B*). MS analysis further verified BODIPY-FA-C12 incorporation into DAG BODIPY-FA-C12/22:0 (corresponding to a mass to charge ratio peak of 832.4 in *SI Appendix*, Fig. S10 *C* and *D*), indicating correct intracellular processing of the internalized BODIPY-labeled FAs for EHD2 +/+ and del/del MEFs. Up to 20 min, no BODIPY-positive TAG species was detected, probably due to short incubation time. However, these data further support our conclusion that loss of EHD2 increases the FA uptake into cells, but not the following FA processing steps.

Decreased EHD2 Expression in Genetic Obesity Models or in Diet-Induced Obesity. Our data indicate an EHD2-dependent control of lipid uptake in adipose tissue, suggesting that EHD2 expression might be dysregulated in obese mice and humans. We therefore investigated if EHD2 expression is altered in two obesity-related mouse models, ob/ob and NZO (40). Indeed, WAT obtained from ob/ob and NZO mice showed reduced EHD2 expression compared to C57BL6/J mice fed by standard diet (Fig. 7*A*). When investigating adipocytes from ob/ob mice, a higher proportion of detached caveolae were found in the obesity mouse model (ratio detached/membrane bound caveolae = 1.4 vs. 0.35 in C57BL6/N mice fed with standard diet) (Fig. 7 *B* and *C*). In addition, we analyzed EHD2 expression in visceral and subcutaneous WAT from patients ranking in their body mass index (BMI) from normal to morbid obesity (BMI < 25 to BMI > 40) (Fig. 7 *D* and *E*). In both depots, EHD2 expression was highest in normal weight subjects and was significantly lower in overweight and obese people whereas EHD2 expression did not differ between different obesity stages. These data imply that EHD2 expression is regulated by lipid uptake and load and suggest that EHD2-mediated caveolar dynamics may be altered in obesity.

Discussion

Here, we identify EHD2 as a negative regulator of caveolae-dependent lipid uptake. Loss of EHD2 resulted in increased LDs in adipose tissue of the whole organism, as well as in cell culture-based experiments. Loss of EHD2 was associated with the detachment of caveolae from the plasma membrane, higher caveolar mobility, and increased FA uptake. We demonstrate that caveolae, the fatty acid translocase CD36, and dynamin-2 play a critical role in the EHD2-dependent lipid uptake pathway. In addition, obese mice and humans exhibit decreased EHD2 expression in WAT. Thus, our study reveals a cell-autonomous, caveolae-dependent lipid uptake route that is controlled by EHD2 and modified by metabolic conditions.

For some time, caveolae have been implicated in lipid uptake. Thus, mice lacking caveolae showed reduced fat mass and did not develop any form of obesity. In addition, Pohl et al. (41) observed decreased oleate uptake after expression of a dominant-negative Cav1 mutant. The EHD2 KO mouse model, described here, revealed the opposite phenotype: e.g., a caveolae gain-of-function in vivo model. In EHD2 KO mice, caveolae were more often detached from the plasma membrane and showed a higher mobility and faster lipid uptake, resulting in enlarged LDs. Unlike in Cav1 overexpressing mice (19), which also show increased FA uptake, the number of caveolae was not increased in EHD2 KO mice. This supports a model in which not only caveolae number, but also caveolar dynamics play a crucial role in this process (Fig. 7*F*). Furthermore, this idea is in line with our structural findings that

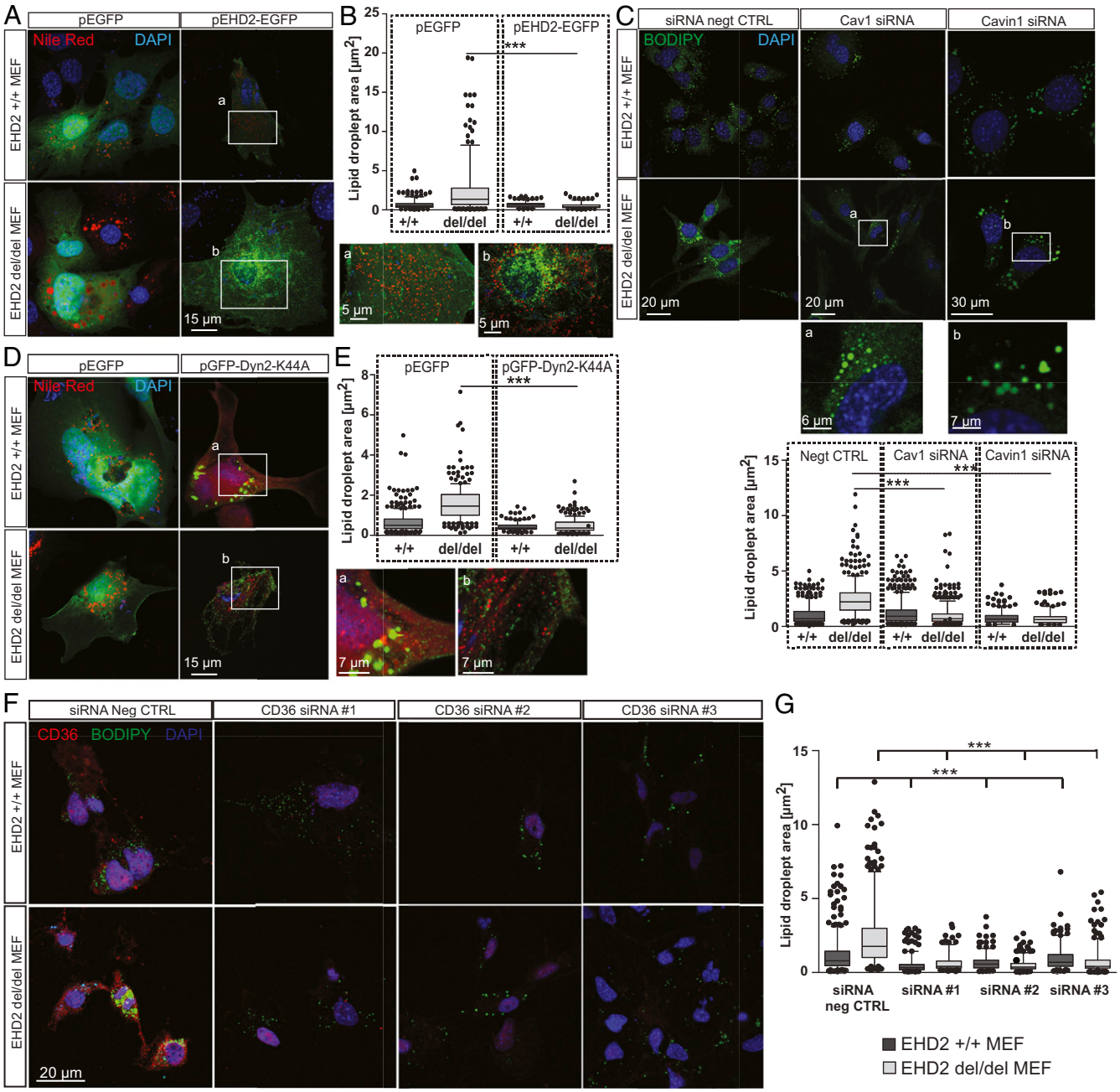

Fig. 5. EHD2-mediated fatty acid uptake depends on Cav1, Cavin 1, Dyn2, and CD36. (*A* and *B*) EHD2 +/+ and del/del MEFs were transfected with either plasmid expressing EGFP (pEGFP) or pEHD2-EGFP, incubated for 48 h, and afterward treated for 6 h with oleic acid, and Nile Red staining was performed to determine LDs [pEGFP: $n(^{+/+}) = 309/3$, n(del/del) = 310/3; pEHD2-EGFP: $n(^{+/+}) = 218/4$, n(del/del) = 184/4]. Boxes *a* and *b* illustrate magnified cell areas. (*C*) EHD2 +/+ and del/del MEFs were treated with Cav1 or Cavin1 siRNA, and LDs were stained with BODIPY [negative control (negt CTRL): $n(^{+/+}) = 504/3$, n(del/del) = 530/3; Cav1 siRNA: $n(^{+/+}) = 521/3$, n(del/del) = 558/3; Cavin1 siRNA: $n(^{+/+}) = 366/3$, n(del/del) = 362/3]. (*D* and *E*) EHD2 +/+ and del/del MEFs were transfected with pGFP-Dyn2-K44A, incubated for 18 h, and afterward treated for 6 h with oleic acid, and Nile Red staining was performed to visualize LDs [pEGFP: $n(^{+/+}) = 309/3$, n(del/del) = 233/4; pGFP-Dyn2-K44A: $n(^{+/+}) = 136/3$, n(del/del) = 237/4]. Boxes *a* and *b* illustrate magnified cell areas. (*F* and *G*) LD size after CD36 siRNA knockdown in EHD2 +/+ and del/del MEFs [G, negative control: $n(^{+/+}) = 584/6$, n(del/del) = 475/6; CD36 siRNA#1: $n(^{+/+}) = 341/3$, n(del/del) = 249/3; CD36 siRNA#2: $n(^{+/+}) = 412/3$, n(del/del) = 468/3; CD36 siRNA#3: $n(^{+/+}) = 251/3$, n(del/del) = 368/3]. The graph illustrates each replicate with mean ± SE; a two-way ANOVA test was used to calculate significance between siRNA negative CTRL and siRNA, and a *t* test was used between $^{+/+}$ and del/del data. Box plots indicate mean ± SE, and single replicates of 5% of maximal and minimum values are illustrated; a *t* test or Mann–Whitney *U* test was used to calculate significance, ***$P < 0.0001$. See also *SI Appendix*, Figs. S7–S9.

EHD2 can form ring-like oligomers that may stabilize the neck of caveolae (24–27), thereby restricting caveolar mobility (21, 22). Based on studies in the EHD2 KO NIH 3T3 cell line, Yeow et al. (42) suggested that EHD1 and/or EHD4 can rescue the loss of EHD2. However, we did not find rescue of caveolae detachment and lipid uptake in EHD2 KO cells by other EHD family members.

The pathway of caveolae-dependent cellular lipid uptake has been intensively studied (4, 19, 20, 33, 34), but the exact molecular mechanisms are still unclear. Our observation indicates that FA uptake depends on caveolar dynamics and detachment, processes which are controlled by EHD2. Indeed, we observed single mobile caveolae loaded with FAs, indicating that caveolae

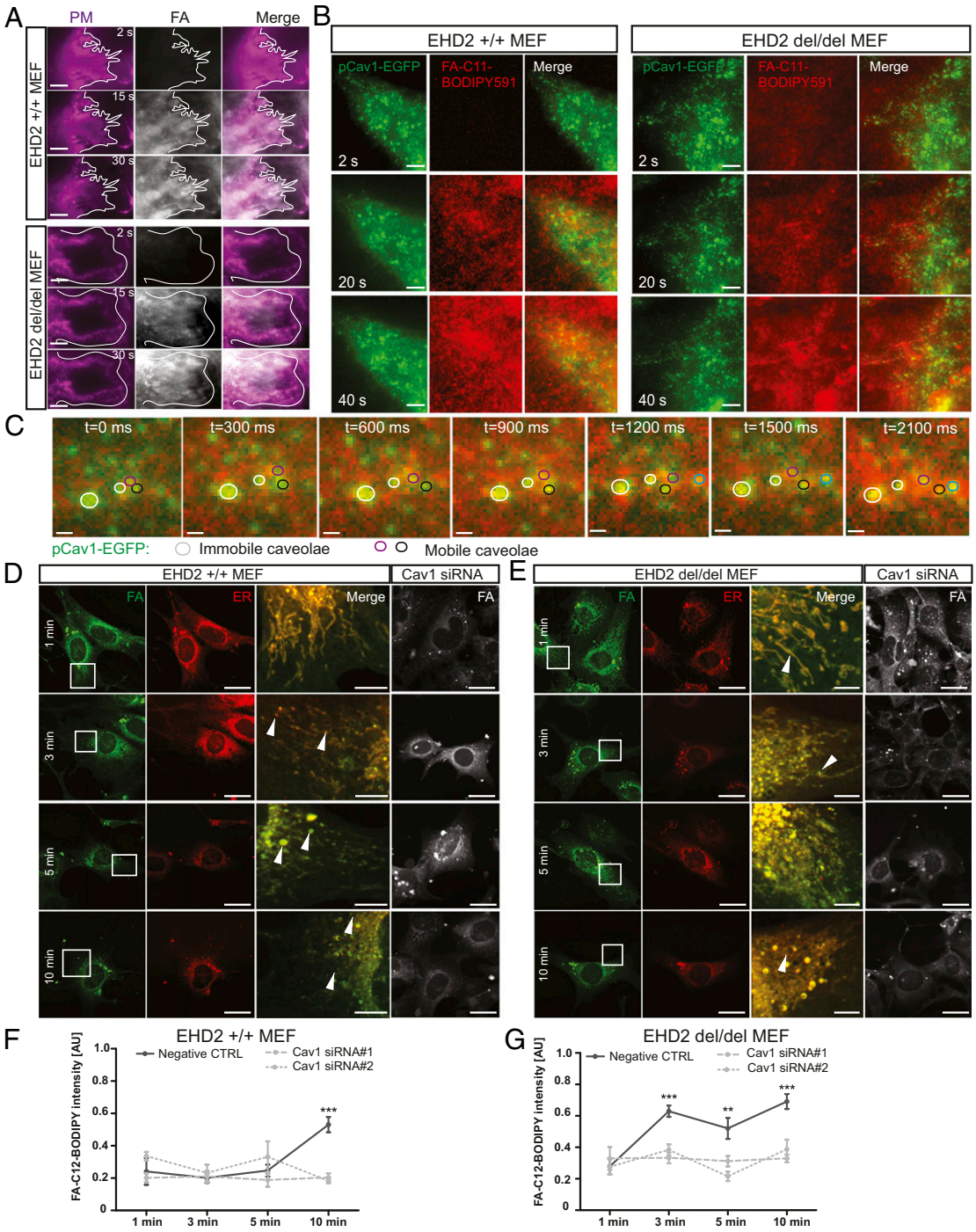

Fig. 6. Caveolae-related fatty acid uptake and trafficking. (*A*) Time-resolved C11-BODIPY591 FA accumulation in the plasma membrane of EHD2 +/+ and del/del MEFs was recorded by TIRF. (Scale bars: 1 μm.) Cell borders are indicated. In both genotypes, FAs intercalated into the plasma membrane within seconds, and no qualitative difference between the two genotypes was observed. (*B* and *C*) Time-resolved TIRF imaging in MEF expressing Cav1-EGFP treated with C11-BODIPY591 FA. (Scale bars: B, 1 μm.) Detailed caveolae movement in EHD2 del/del MEFs treated with C11-BODIPY591 FA (*C*, TIRF imaging, mobile caveolae depicted in black, magenta, and blue circles; immobile caveolae in white circles). (Scale bars: 200 nm.) Single images represent sequential acquisition frames of the recording (see also Movies S9 and S10). (*D* and *E*) C12-BODIPY FA trafficking in EHD2 +/+ (*D*) and del/del (*E*) MEFs treated with Cav1 siRNA (endoplasmic reticulum [ER] stained by ER-TrackerRed). (Scale bars: FA and ER, 20 μm; Merge, 5 μm.) The merged panel illustrates the magnified cell area indicated in the FA panel, and arrowheads indicate LDs. (*F* and *G*) Fluorescence intensity of cellular C12-BODIPY FA [$^{+/+}$: n(Negt CTRL) = 10/3, n(Cav1 si#1) = 12/3, n(Cav1 si#2) = 12/3; del/del: n(Negt CTRL) = 11/3, n(Cav1 si#1) = 12/3, n(Cav1 si#2) = 11/3]. Line graphs indicate mean ± SE. Normal distributed groups were analyzed by *t* test, and not normally distributed values with Mann–Whitney *U* test, $^{**}P < 0.001$, $^{***}P < 0.0001$. PM, plasma membrane; AU, arbitrary unit. See also *SI Appendix*, Fig. S10.

can shuttle FAs from the plasma membrane into the cell. In agreement with previous results (43–45), our analysis of intracellular FA trafficking in MEFs revealed an accumulation of fluorescently labeled FAs in the ER and LDs within minutes. Interestingly, we observed an initial, fast, caveolae-independent and a slower, caveolae-dependent FA uptake. Only the latter was accelerated in the absence of EHD2. It

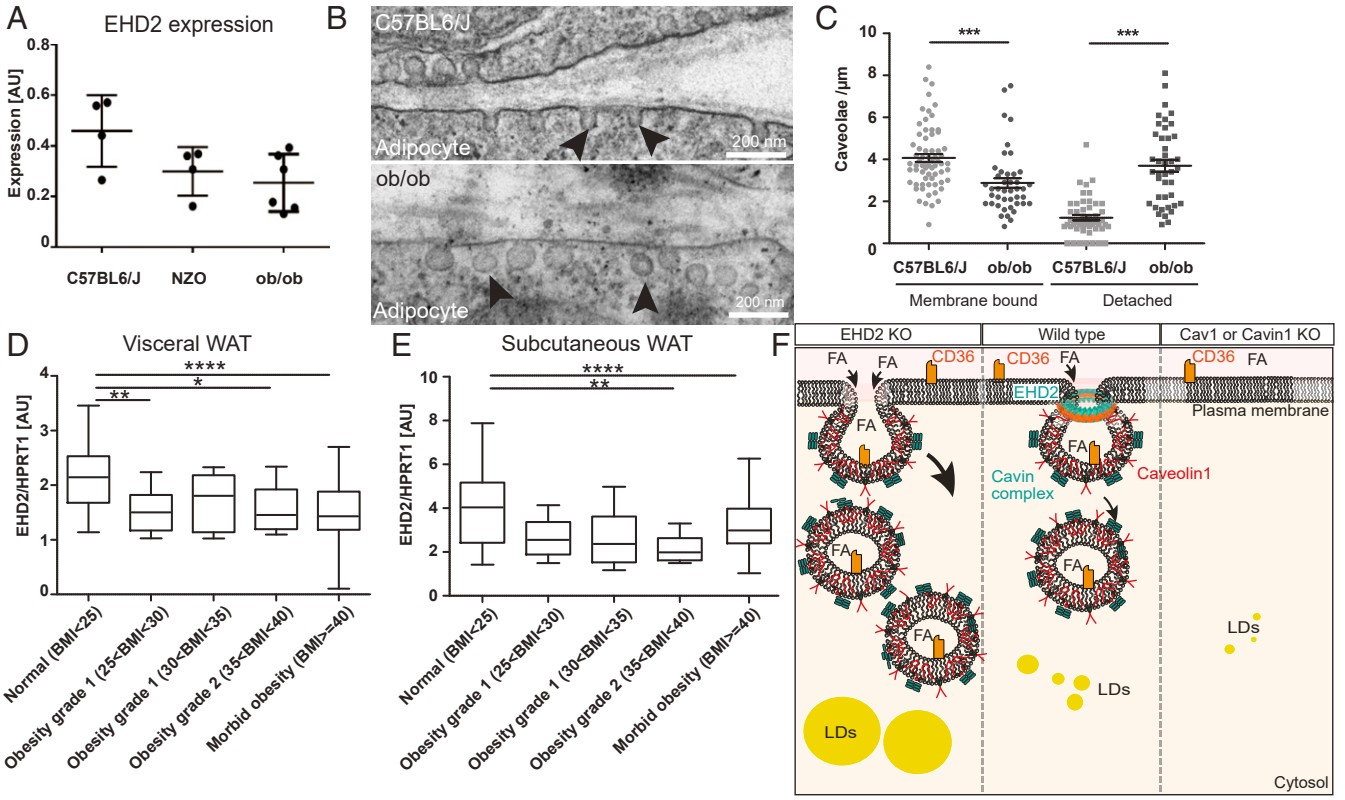

Fig. 7. Decreased EHD2 expression in obesity. (*A*) EHD2 expression level was analyzed in fat tissue of ob/ob or NZO mouse models compared to C57BL6/J mice ($n = 5$). (*B* and *C*) Investigation of caveolae by EM [n(ob/ob mice) = 85/2; n(C57BL6/N) = 117/2]. Black arrowheads indicate caveolae. (*D* and *E*) EHD2 expression in visceral (*E*) or subcutaneous WAT (*F*) in obese patients [n(normal) = 31; n(overweight) = 23; n(obesity grade 1) = 7; n(obesity grade 2) = 17; n(obesity grade 3) = 202]. (*F*) The model illustrates how FA uptake is affected by caveolae function. In the absence of caveolae, FA uptake is reduced, resulting in smaller LDs compared to normal conditions. In the absence of EHD2, FA is increased, suggesting a regulatory function of EHD2 in caveolae-dependent lipid uptake. FFA, free fatty acid; LD, lipid droplet. Box plots indicate median with whiskers from maximal to minimum value, or each replicate with mean ± SE is represented. Normal distributed groups were analyzed by *t* test, and not normally distributed values with Mann–Whitney *U* test, $*P < 0.05$, $**P < 0.001$, $***P < 0.0001$, $****P < 0.00001$.

remains elusive how caveolae precisely shuttle FAs to the ER and/or LDs and whether adipose cells may adopt specialized features in their lipid trafficking pathway compared to MEFs. The EHD2 knockout mouse model will be a useful tool to further dissect the molecular mechanisms of caveolae-dependent lipid uptake in various tissues.

The loss of EHD2 on the cellular level led to increased fat deposits on the organismic level, which was particularly evident in older animals. The observed phenotype based on the global loss of EHD2 could be influenced by organ cross-talk (46). However, we did not find any evidence for differences in adipocyte-derived secretory factors, such as leptin (*SI Appendix*, Fig. S4). Furthermore, increased lipid uptake was dependent on caveolae, as shown by Cav1 and Cavin1 knockdown experiments, and LD growth could specifically be induced by viral infection of Cre recombinase in EHD2 cKO flox/flox, but not in flox/wild type adipocytes. Thus, increased lipid uptake is caused by a cell-autonomous, caveolae-dependent mechanism. Morén et al. (30) observed a decreased LD size in differentiated 3T3-L1 cells that were treated with EHD2 siRNA 4 d after initial differentiation. However, we observed increased LD size when EHD2 was silenced as described in Morén et al. (30) or during the entire differentiation process. The cause of this apparent discrepancy is unclear, but, given the wealth of data from various cell types and cell lines described in the current study, we are convinced that EHD2 loss generally leads to increased lipid droplet size.

Despite the increased LDs in mice lacking EHD2, the body weight and triglyceride content of EHD2 del/del and EHD2 del/+ mice were similar. This suggests alterations in LD biogenesis, but not in triglyceride storage itself in the absence of EHD2. Indeed, FA processing steps appeared similar in EHD2 lacking MEFs (*SI Appendix*, Fig. S10). In line with the latter and consistent with our fatty acid uptake experiments, we observed increased cellular free FA levels in the absence of EHD2, at least in the first 24 h upon exposure to high fatty acid concentrations. Compared to triglycerides, EHD2-lacking BAT and MEFs showed slightly increased cholesterol and cholesterol ester concentrations. This is a particularly interesting as caveolae are enriched in cholesterol, and the increased uptake of caveolae in EHD2 del/del cells may therefore concurrently lead to increased cholesterol uptake. In line with the increased FA uptake rates and LD sizes, we observed up-regulation of LD biogenesis genes, like Perilipin1 or DGAT2. Intracellular FAs are known to activate the transcription factor PPARγ (47–49), which, in addition, tended to be up-regulated in EHD2-lacking tissue. Consequently, PPARγ may induce the transcription of various adipogenic and LD-related genes, as observed in our expression analyses.

EHD2 del/del WAT and cultivated EHD2 del/del adipocytes showed reduced expression levels of genes involved in de novo lipogenesis, like SREBP1 or FAS. Similar compensatory mechanisms were noted in patients suffering from obesity (50–52). Remarkably, the expression levels of EHD2 were strongly reduced in WAT from obese patients, as well as in WAT of two obese mouse models (ob/ob and NZO mice). Thus, expression of EHD2 appears to negatively correlate with adipocyte size, therefore reflecting the situation in the EHD2 KO mouse (see also ref. 53). We speculate that an imbalance in number, lifetime, and

mobility of caveolae may accompany the development and progression of obesity.

Methods

Please see *SI Appendix, SI Materials and Methods* for a detailed description of all materials and methods. The datasets generated and analyzed during the current study are available from the corresponding author on reasonable request.

EHD2 Delta E3 Mouse Strain Generation. The EHD2 targeting construct was generated by insertion of two loxP sequences flanking exon 3 of EHD2 genomic DNA by homologous recombination in *Escherichia coli* as previously described (54), including a pGK Neomycin and a diphtheria toxin A (DTA) cassette. Electroporation of the linearized targeting vector in R1 embryonic stem cells was performed. Mice carrying a loxP-flanked exon 3 of the EHD2 gene were mated to Cre deleter mice to generate EHD2 mutant (del/del) mice. After backcrossing the EHD2 del/del mice with C57BL6/N (Charles River, male) for six generations, only male EHD2 del/del or EHD2 del/+ mice were used. All animals were handled according to governmental animal welfare guidelines and were housed under standard conditions.

Human EHD2 Expression. All regulated procedures carried out on animals involved in this publication were applied for and approved by the Landesamt für Gesundheit und Soziales (LAGeSo, State of Berlin) and were in full compliance with German and European Union animal protection laws. The study was approved by the Ethics Committee of the University of Leipzig (approval no. 159-12-21052012), and performed in accordance to the declaration of Helsinki. All subjects gave written informed consent before taking part in this study. Samples were treated as previously described (55).

ACKNOWLEDGMENTS. We thank Petra Stallerow for taking care of the EHD2 delta E3 mouse strain, Karin Jacobi for advice with the animal applications, Vivian Schulz and Carola Bernert for helping with the genotyping of the mice, Claudio Shah for purifying the EHD2 antiserum, Christian Lüchtenborg for MS-based lipid analysis, and the advanced light imaging facility at the Max Delbrück Center for technical support. The authors acknowledge financial support from Deutsche Forschungsgemeinschaft (DFG) Grants SFB 958/A7 (to V.H.), SFB 958/A12 (to O.D.), and SFB 958/A13 (to A.S.) and Project 278001972-TRR 186 (to H.O. and B.B.), and support by The Initiative and Networking Fund of the Helmholtz Association.

1. J. P. X. Cheng, B. J. Nichols, Caveolae: One function or many? *Trends Cell Biol.* **26**, 177–189 (2016).
2. B. Sinha *et al.*, Cells respond to mechanical stress by rapid disassembly of caveolae. *Cell* **144**, 402–413 (2011).
3. S. Torrino *et al.*, EHD2 is a mechanotransducer connecting caveolae dynamics with gene transcription. *J. Cell Biol.* **217**, 4092–4105 (2018).
4. L. Liu *et al.*, Deletion of Cavin/PTRF causes global loss of caveolae, dyslipidemia, and glucose intolerance. *Cell Metab.* **8**, 310–317 (2008).
5. H. Ju, R. Zou, V. J. Venema, R. C. Venema, Direct interaction of endothelial nitric-oxide synthase and caveolin-1 inhibits synthase activity. *J. Biol. Chem.* **272**, 18522–18525 (1997).
6. A. Ludwig *et al.*, Molecular composition and ultrastructure of the caveolar coat complex. *PLoS Biol.* **11**, e1001640 (2013).
7. A. Ludwig, B. J. Nichols, S. Sandin, Architecture of the caveolar coat complex. *J. Cell Sci.* **129**, 3077–3083 (2016).
8. M. Stoeber *et al.*, Model for the architecture of caveolae based on a flexible, net-like assembly of Cavin1 and Caveolin discs. *Proc. Natl. Acad. Sci. U.S.A.* **113**, E8069–E8078 (2016).
9. J. Mohan, B. Morén, E. Larsson, M. R. Holst, R. Lundmark, Cavin3 interacts with cavin1 and caveolin1 to increase surface dynamics of caveolae. *J. Cell Sci.* **128**, 979–991 (2015).
10. O. Kovtun, V. A. Tillu, N. Ariotti, R. G. Parton, B. M. Collins, Cavin family proteins and the assembly of caveolae. *J. Cell Sci.* **128**, 1269–1278 (2015).
11. C. G. Hansen, G. Howard, B. J. Nichols, Pacsin 2 is recruited to caveolae and functions in caveolar biogenesis. *J. Cell Sci.* **124**, 2777–2785 (2011).
12. Y. Senju, Y. Itoh, K. Takano, S. Hamada, S. Suetsugu, Essential role of PACSIN2/syndapin-II in caveolae membrane sculpting. *J. Cell Sci.* **124**, 2032–2040 (2011).
13. E. Seemann *et al.*, Deciphering caveolar functions by *syndapin III* KO-mediated impairment of caveolar invagination. *eLife* **6**, e29854 (2017).
14. M. Drab *et al.*, Loss of caveolae, vascular dysfunction, and pulmonary defects in caveolin-1 gene-disrupted mice. *Science* **293**, 2449–2452 (2001).
15. M. M. Hill *et al.*, PTRF-Cavin, a conserved cytoplasmic protein required for caveola formation and function. *Cell* **132**, 113–124 (2008).
16. B. Razani *et al.*, Caveolin-1-deficient mice are lean, resistant to diet-induced obesity, and show hypertriglyceridemia with adipocyte abnormalities. *J. Biol. Chem.* **277**, 8635–8647 (2002).
17. S. Martin *et al.*, Caveolin-1 deficiency leads to increased susceptibility to cell death and fibrosis in white adipose tissue: Characterization of a lipodystrophic model. *PLoS One* **7**, e46242 (2012).
18. S. Y. Ding *et al.*, Pleiotropic effects of cavin-1 deficiency on lipid metabolism. *J. Biol. Chem.* **289**, 8473–8483 (2014).
19. N. Briand *et al.*, Caveolin-1 expression and cavin stability regulate caveolae dynamics in adipocyte lipid store fluctuation. *Diabetes* **63**, 4032–4044 (2014).
20. J. Pohl *et al.*, Long-chain fatty acid uptake into adipocytes depends on lipid raft function. *Biochemistry* **43**, 4179–4187 (2004).
21. B. Morén *et al.*, EHD2 regulates caveolar dynamics via ATP-driven targeting and oligomerization. *Mol. Biol. Cell* **23**, 1316–1329 (2012).
22. M. Stoeber *et al.*, Oligomers of the ATPase EHD2 confine caveolae to the plasma membrane through association with actin. *EMBO J.* **31**, 2350–2364 (2012).
23. M. Uhlén *et al.*, Tissue-based map of the human proteome. *Science* **347**, 1260419 (2015).
24. O. Daumke *et al.*, Architectural and mechanistic insights into an EHD ATPase involved in membrane remodelling. *Nature* **449**, 923–927 (2007).
25. C. Shah *et al.*, Structural insights into membrane interaction and caveolar targeting of dynamin-like EHD2. *Structure* **22**, 409–420 (2014).
26. M. Hoernke *et al.*, EHD2 restrains dynamics of caveolae by an ATP-dependent, membrane-bound, open conformation. *Proc. Natl. Acad. Sci. U.S.A.* **114**, E4360–E4369 (2017).
27. A. A. Melo *et al.*, Structural insights into the activation mechanism of dynamin-like EHD ATPases. *Proc. Natl. Acad. Sci. U.S.A.* **114**, 5629–5634 (2017).
28. E. Shvets, V. Bitsikas, G. Howard, C. G. Hansen, B. J. Nichols, Dynamic caveolae exclude bulk membrane proteins and are required for sorting of excess glycosphingolipids. *Nat. Commun.* **6**, 6867–6883 (2015).
29. D. L. Brasaemle, G. Dolios, L. Shapiro, R. Wang, Proteomic analysis of proteins associated with lipid droplets of basal and lipolytically stimulated 3T3-L1 adipocytes. *J. Biol. Chem.* **279**, 46835–46842 (2004).
30. B. Morén *et al.*, EHD2 regulates adipocyte function and is enriched at cell surface-associated lipid droplets in primary human adipocytes. *Mol. Biol. Cell* **30**, 1147–1159 (2019).
31. J. M. Rutkowski, J. H. Stern, P. E. Scherer, The cell biology of fat expansion. *J. Cell Biol.* **208**, 501–512 (2015).
32. F. Wilfling *et al.*, Triacylglycerol synthesis enzymes mediate lipid droplet growth by relocalizing from the ER to lipid droplets. *Dev. Cell* **24**, 384–399 (2013).
33. A. Ring, S. Le Lay, J. Pohl, P. Verkade, W. Stremmel, Caveolin-1 is required for fatty acid translocase (FAT/CD36) localization and function at the plasma membrane of mouse embryonic fibroblasts. *Biochim. Biophys. Acta* **1761**, 416–423 (2006).
34. J. Pohl, A. Ring, W. Stremmel, Uptake of long-chain fatty acids in HepG2 cells involves caveolae: Analysis of a novel pathway. *J. Lipid Res.* **43**, 1390–1399 (2002).
35. P. F. Pilch, T. Meshulam, S. Ding, L. Liu, Caveolae and lipid trafficking in adipocytes. *Clin. Lipidol.* **6**, 49–58 (2011).
36. Z. Li *et al.*, A novel Rab10-EHBP1-EHD2 complex essential for the autophagic engulfment of lipid droplets. *Sci. Adv.* **2**, e1601470 (2016).
37. P. Oh, D. P. McIntosh, J. E. Schnitzer, Dynamin at the neck of caveolae mediates their budding to form transport vesicles by GTP-driven fission from the plasma membrane of endothelium. *J. Cell Biol.* **141**, 101–114 (1998).
38. N. S. Eyre, L. G. Cleland, N. N. Tandon, G. Mayrhofer, Importance of the carboxyl terminus of FAT/CD36 for plasma membrane localization and function in long-chain fatty acid uptake. *J. Lipid Res.* **48**, 528–542 (2007).
39. N. Aboulaich, J. P. Vainonen, P. Strålfors, A. V. Vener, Vectorial proteomics reveal targeting, phosphorylation and specific fragmentation of polymerase I and transcript release factor (PTRF) at the surface of caveolae in human adipocytes. *Biochem. J.* **383**, 237–248 (2004).
40. M. Kleinert *et al.*, Animal models of obesity and diabetes mellitus. *Nat. Rev. Endocrinol.* **14**, 140–162 (2018).
41. J. Pohl, A. Ring, U. Korkmaz, R. Ehehalt, W. Stremmel, FAT/CD36-mediated long-chain fatty acid uptake in adipocytes requires plasma membrane rafts. *Mol. Biol. Cell* **16**, 24–31 (2005).
42. I. Yeow *et al.*, EHD proteins cooperate to generate caveolar clusters and to maintain caveolae during repeated mechanical stress. *Curr. Biol.* **27**, 2951–2962.e5 (2017).
43. W. Stremmel, L. Pohl, A. Ring, T. Herrmann, A new concept of cellular uptake and intracellular trafficking of long-chain fatty acids. *Lipids* **36**, 981–989 (2001).
44. M. J. McArthur *et al.*, Cellular uptake and intracellular trafficking of long chain fatty acids. **40**, 1371–1383 (1999).
45. D. G. Mashek, R. A. Coleman, Cellular fatty acid uptake: The contribution of metabolism. *Curr. Opin. Lipidol.* **17**, 274–278 (2006).
46. J. H. Stern, J. M. Rutkowski, P. E. Scherer, Adiponectin, leptin, and fatty acids in the maintenance of metabolic homeostasis through adipose tissue crosstalk. *Cell Metab.* **23**, 770–784 (2016).
47. T. Varga, Z. Czimmerer, L. Nagy, PPARs are a unique set of fatty acid regulated transcription factors controlling both lipid metabolism and inflammation. *Biochim. Biophys. Acta* **1812**, 1007–1022 (2011).
48. M. I. Lefterova, A. K. Haakonsson, M. A. Lazar, S. Mandrup, PPARγ and the global map of adipogenesis and beyond. *Trends Endocrinol. Metab.* **25**, 293–302 (2014).
49. U. A. White, J. M. Stephens, Transcriptional factors that promote formation of white adipose tissue. *Mol. Cell. Endocrinol.* **318**, 10–14 (2010).
50. E. Guiu-Jurado *et al.*, Downregulation of de novo fatty acid synthesis in subcutaneous adipose tissue of moderately obese women. *Int. J. Mol. Sci.* **16**, 29911–29922 (2015).
51. L. Eissing *et al.*, De novo lipogenesis in human fat and liver is linked to ChREBP-β and metabolic health. *Nat. Commun.* **4**, 1528–1539 (2013).
52. G. Solinas, J. Borén, A. G. Dulloo, De novo lipogenesis in metabolic homeostasis: More friend than foe? *Mol. Metab.* **4**, 367–377 (2015).
53. S. B. Sonne *et al.*, Obesity is associated with depot-specific alterations in adipocyte DNA methylation and gene expression. *Adipocyte* **6**, 124–133 (2017).
54. P. Liu, N. A. Jenkins, N. G. Copeland, A highly efficient recombineering-based method for generating conditional knockout mutations. *Genome Res.* **13**, 476–484 (2003).
55. E. Guiu-Jurado *et al.*, Bone morphogenetic protein 2 (BMP2) may contribute to partition of energy storage into visceral and subcutaneous fat depots. *Obesity (Silver Spring)* **24**, 2092–2100 (2016).